International Conference on Mechanical System Engineering and Technology Applications (ICoMSETA) 2024, pp. X – XX

Microstructural Insight of Cold-Deformed Bimetallic Structures Produced via WAAM

Zarirah Karrim Wani[1], Ahmad Baharuddin Abdullah* and Zuhailawati Hussain[2]

[1]Metal Forming Lab, School of Mechanical Engineering, Universiti Sains Malaysia, 14300 Nibong Tebal, Pulau Pinang, Malaysia
[2] School of Mineral Materials and Mineral Resources Engineering, Universiti Sains Malaysia, 14300, Nibong Tebal, Pulau Pinang

*E-mail: mebaha@usm.my

Abstract. This study investigates the microstructural evolution and interlayer bonding in term of interfacial reaction for bimetallic interfaces fabricated through wire arc additive manufacturing (WAAM), focusing on ER70s-6 and ER308L materials. Utilizing optical microscope (OM), scanning electron microscopy (SEM) and energy-dispersive X-ray spectroscopy (EDS/EDAX), this research investigates the effects of cold deformation on surface morphology and elemental diffusion within each parent metal. The study addresses the crucial need for understanding and utilizing the WAAM process, as well as selecting suitable materials and parameters to achieve robust interlayer bonding, which is essential for ensuring component quality and integrity. By uncovering fundamental mechanisms governing bimetallic bonding under cold deformation, this research contributes to advancing additive manufacturing technologies and enhancing the performance and reliability of manufactured components across diverse industrial sectors.

Keywords: Wire Arc Additive Manufacturing, Cold forging, Bimetallic.

1. Introduction

The concept of bimetallic bonding in wire arc additive manufacturing (WAAM) involves the joining of two different metallic materials to form a single component or structure using the WAAM process. WAAM is an additive manufacturing technique that utilises an electric arc to melt and deposit metal wire onto a substrate, layer by layer, to build up the desired shape [1]. In this approach, a layer of one metal is deposited on a substrate, followed by a layer of another metal on top. The interface between the two materials forms when subsequent layers are added, creating a bimetallic interlayer. It allows for the combination of different materials with complementary properties such as strength [2], corrosion resistance [3,4], and conductivity. Bimetallic materials offer numerous advantages and superior performance compared to single materials [5]. For example, the combination of copper and stainless steel [6] offers advantages for their combinations when copper offers better thermal and electrical conductivity, whereas stainless steel is stronger, more durable, and resistant to corrosion. The resulting

bimetallic component gains the improved thermal and electrical capabilities of copper and the strength and corrosion resistance of stainless steel when these materials are joined via WAAM. The bimetallic structure is very useful for applications in the electronics, automotive, and aircraft sectors where both mechanical robustness and effective thermal or electrical conductivity are essential.

Researchers can modify the material characteristics to match certain performance requirements for different applications by carefully choosing and mixing metals. There is some other mixing for bimetallic structures such as ER70s-6 – ER308LSi [7], ER70s-6-SS316L [8], AISI 316L SS and Cu [6], ER70s-6-R309LS [2], ER70s-6-SS316L [9], and ER70s-6-NiCr [10], and SS308L-Inconel 718 [11]. Besides mixing wires for bimetallic WAAM, wires are also combined with substrates made from various other materials. The mixing of ER70s-6 with the substrate, S355 as a bimetal joint demonstrated by Zhai et al, shows a strong bonding and fusing at the interface in the microstructural analysis [12]. Research by Chen et al. [13] demonstrates the fabrication of a bimetallic laminated steel structure (BLSS) by alternately depositing 304 stainless steel (SS 304) and low carbon steel (ER70s-6) onto a Q345 substrate. The microstructure of the BLSS shows that the SS304 layer contained martensite, unlike the single SS30 structure, which had vermicular ferrite in an austenite matrix, while the ER70s-6 layer remained largely unchanged compared to the single ER70s-6 structure. The results also show the fine grains formed at the interface between the ER70s-6 and 304 SS layers. To achieve high geometric precision and excellent mechanical properties near the parent metal, it requires optimal parameter settings for each material system and post-processing [14].

Cold deformation is one example of a post-processing treatment that enhances the properties of metal. Cold deformation is the process of modifying the size or shape of a material below its recrystallization temperature. Cold rolling, cold drawing, or cold forging are a few examples of cold deformation. There are numerous advantages for the materials that undergo cold deformation especially in the microstructure [15]. The grain size inside the material's microstructure usually decreases after it undergoes a cold deformation process. Dislocations and other crystal structural flaws are introduced during cold deformation, which increases the strength, hardness, and stiffness of the material. For applications needing outstanding mechanical performance, such as those in the automotive, aerospace, and construction sectors, this makes cold-deformed materials extremely desirable [16]. Cold working is useful for making precision components of constant quality due to the homogeneous deformation and tight tolerances it allows. Few researchers study WAAM and use forging as a post-treatment procedure to enhance the materials' mechanical qualities and microstructure. Experiments conducted using single material and involving forging have revealed valuable findings from prior research. Duarte et al. [17] combine WAAM with in-situ hot forging using a custom hammer to forge the deposited bead for AISI316L stainless steel wire on a mild steel substrate. The findings additionally support the notion that this innovative hot forging WAAM variation facilitates a decrease in grain size, leading to heightened grain boundary density and consequent enhancements in mechanical properties. Other than hot forging, cold forging has been used to forge WAAM parts made of AA4043 metal fabricated using the TIG welding technique, as conducted by Ajwad et al. [18]. The finding reveal that the forged specimen has elongated grain compared to the pre-forged image. Parvaresh et al. investigated the impact of inter-layer cold forging on the microstructure and mechanical properties of AISI 347 structures made by WAAM, as opposed to in-situ or post-build forging [19]. The inter-layer cold forging significantly shows the refining of the grain structure through recrystallization. Combining bimetallic WAAM with deformation processes like forging offers a new way to create a high-performance structure. This method enhances mechanical properties and allows for tailored microstructures. In this integrated manufacturing process, bimetallic structures are initially fabricated using WAAM, followed by cold deformation; forging to further refine the microstructure and shape the component to its final form. Several industries utilise bimetallic WAAM for a variety of applications due to its versatility, customisation capabilities, and potential for cost-effective production. Bimetallic WAAM usually used in aerospace [20] for manufacturing lightweight yet robust components, such as engine parts, structural components, and heat exchangers. The ability to combine different metals with complementary properties allows for the production of components with optimised performance and reduced weight [21].

This research focusses on the manufacturing of bimetal structures utilising ER70s-6 mild steel and ER308L stainless steel. Stainless steel offers great tensile strength, excellent corrosion resistance, and

good toughness at low temperatures, while mild steel is recognized for its good tensile strength, ductility, and impact resistance. For components exposed to seawater in maritime applications, combining mild steel with stainless steel ensures corrosion resistance and structural integrity. In addition to the previously mentioned applications, this combination of ER70S-6 and ER308L is also utilized in the food processing industry to construct mixing tanks and conveyors. In these applications, mild steel is chosen for its cost-effectiveness and strength, while stainless steel is used for its hygienic properties and corrosion-resistant interior surfaces that come into contact with food. However, we haven't reached the stage of measuring strength and other performance factors yet. Our initial focus is on understanding the microstructural insights of the combination through additional cold forging. Therefore, in this investigation, we are not measuring strength or corrosion resistance. Previous research by Ayan et al. [7] utilized the same materials as this study but applied different deposition styles and parameters. Moreover, their investigation did not include forging on the fabricated functionally graded material structure. This study seeks to address the existing gap in the literature on the microstructural characteristics of bimetal WAAM by incorporating cold forging into the fabricated bimetal structure.

2. Materials and method

The experiment was carried out using a custom CNC machine with a MIG welding torch attached to it. There are three reconfigurable system installed on this machine, including MIG welding machine, a modified CNC machine and an open-source programming software (GRBL). An ACO MIG 200J machine was used to deposit a 0.8 mm diameter ER70s-6 mild steel (MS) and ER308L stainless steel (SS) on a square aluminium substrate, Al6061, with a 100 x 100 mm dimension. The first layer deposited is the ER308L and the next layer is the ER70s-6 wire. The length of the produced samples was fixed at 50 mm. The width preferred for both wires in this experiment is 10 mm. A one-way deposition strategy was adopted, wherein the torch always returned to the same starting point before starting the new layer as shown in Figure 1. The welding torch supplied the shielding gas and wire from the welding machine. The chemical composition of both wires is shown in Table 1. To obtain the preferred width for the deposited bead, the parameters for wire feed rate and travel speed are set differently according to the previous experiment data setting. This is because the bead size depends on the setting of welding parameters, especially the wire feed rate and travel speed [26]. The type of shielding gas is also different for both wires, where carbon dioxide gas is used for MS and Argon gas used for SS. However, the shielding gas rate is fixed for both wires at 10 L/min. The set of WAAM processing parameters used to deposit both types of wires is shown in Table 2. Six samples were produced to study the effect of cold forging + WAAM: three as-built samples (non-forge) and the other three samples with a cold forging process with a reduction of 5 mm from the actual height of the bead.

Table 1: Chemical composition of MS and SS welding wires

Weight%	**C**	**Mn**	**Si**	**P**	**S**	**Ni**	**Cr**	**Mo**	**V**	**Cu**
Mild steel, ER 70s-6	0.06-0.15	1.40-1.85	0.80-1.15	0.025 max	0.035 max	0.15 max	0.15 max	0.15 max	0.03 max	0.50 max

Weight%	C	Mn	Si	Cr	Ni	S	P	Mo	Cu
Stainless steel, ER 308L	0.03	1-2.5	0.30-0.65	19.5-22	9-11	0.03 max	0.03 max	0.75 max	0.75 max

Table 2: WAAM process parameters for deposited types of wires

	Mild steel, ER70s-6	**Stainless steel, ER308L**
Wire Feed Rate, WFR (mm/sec)	81.6	81.6
Travel Speed, TS (mm/min)	80	50
Shielding Gas	100 % CO_2	100 % Ar

Shielding Gas Flow Rate (L/min)	10	10

The deposited bead was later detached from the aluminium substrate. Cold forging was performed on three samples using a 100 tonne mechanical press. The specimen was forged from the top surface (MS bead), reducing the actual wall height by 5 mm. The 5 mm reduction was set using a dial gauge. The specimens were then cut at the centre using a metallurgical cutter to observe the joining of the two different materials inside the built wall.

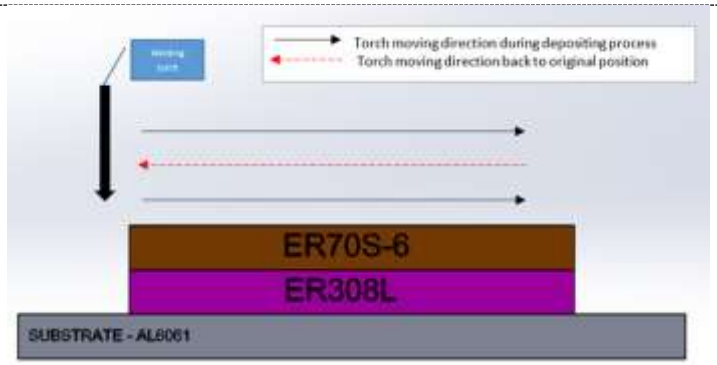

Figure 1. Depositing direction

Next, the specimen preparation involved surface mounting, grinding, polishing, and etching. A 2% Nital solution was used to etch the MS zone, while a Carpenter etchant (ferric chloride, cupric chloride, ethanol, hydrochloric acid, nitric acid) was used for the SS zone. Microstructure observation was performed using a micro visual optical microscope, XOPTRON X80 series and a S-3400N model for Scanning Electron Microscope (SEM). SEM with Energy Dispersive X-ray Spectrometry (EDS) was used to study how chemical elements mix in the parent metal. EDS detects X-rays given off by the sample when hit by the SEM's electron beam. Each element emits X-rays with unique energies when excited, which helps identify and measure the elements in the sample.

3. Result and discussions

3.1. Microstructure evolution

3.1.1. Interlayer zone

In the context of WAAM, the area where two subsequent layers of material are fused together and deposited is referred to as the interlayer zone. In Figures 2a, 2b, 3a and 3b, the SEM and OM image of the interlayer zone shows the deposited bead of MS on the SS. The deposited bead was observed to have an irregular shape. The irregularities in surface and shape can be attributed to the fundamental challenges of thermally bonding diverse materials. In research conducted by Kabaldin et al., MS (ER70s-6) and SS (ER309LSi) were joined using hybrid technology, incorporating a milling process after depositing the first material [2]. In his studies, the second material was then deposited on the milled bead. However, this process resulted in irregularities on the deposited bead, as shown in Figure 4. Despite milling the bead, these irregularities persisted, indicating the necessity of optimising the parameters for the deposition of the second material. The method of transporting the surfacing material to the weld pool is crucial, as it influences the technological printing modes, which in turn affect the geometrical parameters of the workpiece according to the WAAM process. A close-up of the interlayer zone for both forged and non-forged shows that while some parts are well joined, others have defects. This joining issue [22] might be due to some reason such as, uneven heat distribution, difference thermal expansion, improper process parameter and etc. Kabaldin et al. identified the primary causes of such defects as differences in the physical characteristics of the attached materials, including phase transitions, linear expansion coefficient, thermal conductivity, melting temperature, and crystal lattice types [2]. Pereira also

observed a lack of fusion at the joining zone when MS (ER70s-6) was joined with a substrate of S235JR, revealing a typical low-carbon steel microstructure with a ferrite matrix and a minor amount of secondary pearlite phase, which is expected given the rapid solidification conditions of the WAAM process and the low carbon content [23]. Another reason for poor joining in some areas is the presence of impurities or contaminants on the surface of the first bead. If the first bead is not properly cleaned before depositing the second layer, it can result in weak bonds and defects.

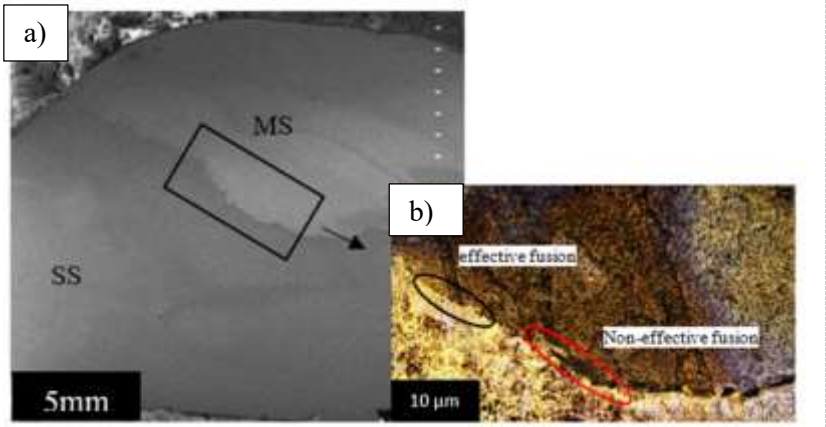

Figure 2. Interlayer zone images for forged specimen a) SEM image and b) OM image

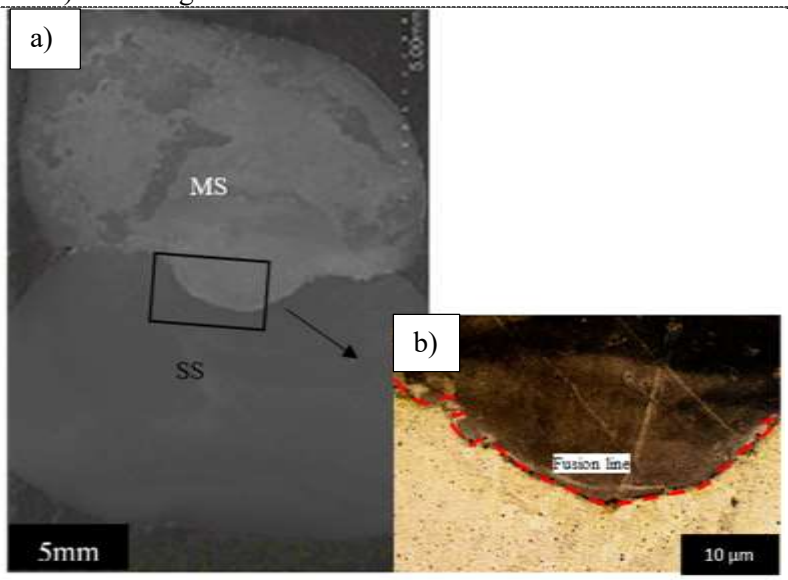

Figure 3. Interlayer zone images for non-forge specimens a) SEM image and b) OM image

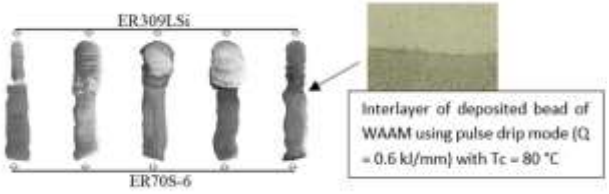

Figure 4. Irregular bead show when depositing SS on the MS with different heat input set up [2]

3.1.2. MS and SS zone

The different microstructure images founded in MS and SS zone for both forge and non-forge bimetallic specimens are depicted in Figure 5. The elongation and compact structure in the Figure 5a and 5b indicate grain deformation during the cold deformation post-treatment for the MS zone. The noticeable changes in grain shapes and structure observed in the MS zone compared to the SS zone are likely due to the forging process being conducted directly on the MS bead. The grains are compressed from a relatively circular shape to an irregular, elongated shape. The simpler metallurgical composition of MS, primarily composed of iron and carbon, contrasts with SS, which contains chromium, nickel, and other alloying elements. This difference causes the grain size and structure in the forged area to change. Figure 5c shows an image near the interlayer zone, while Figure 5d captures the centre of the SS zone in the bimetallic specimen. The typical MS and SS microstructures without the forging process are presented to validate the non-forged specimens. An ER316L specimen undergoing WAAM with hybrid hot forging using various hammer designs results in different microstructures. The as-built and hot-forged microstructures show differences in grain sizing and dendrite size [17]. This effect is similar to that of the cold forging application, but cold forging offers additional advantages, particularly in terms of cost.

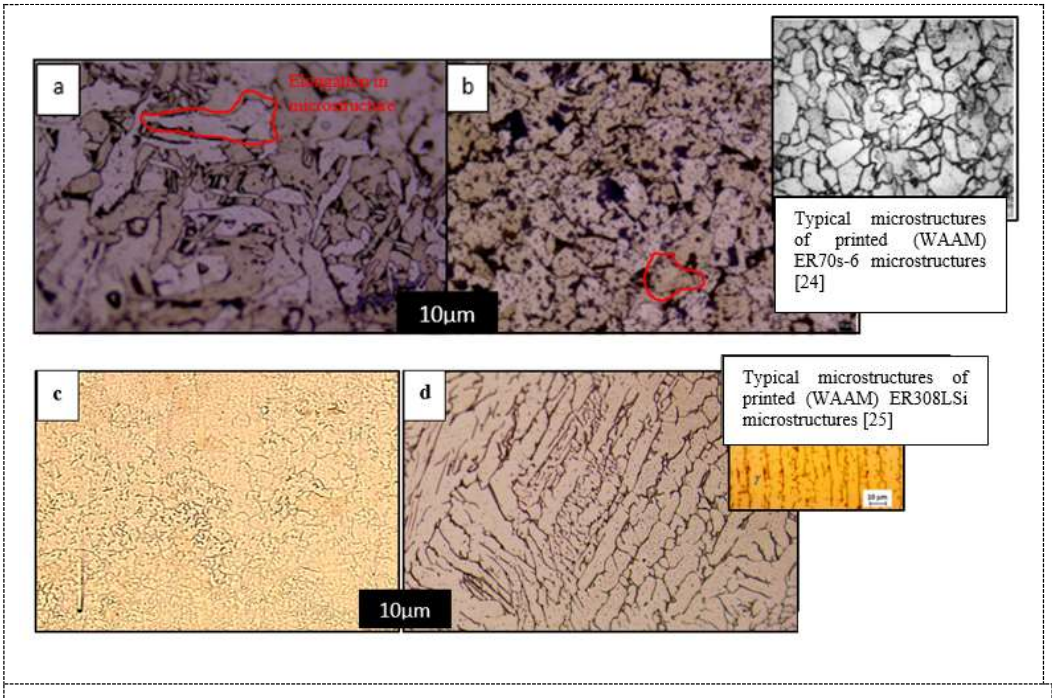

Figure 5. MS zone; (a) forged, (b) non-forge and SS zone; (c) forged, (d)non-forged

3.2. EDAX discussions

Figures 6 and 7 illustrate the EDAX data for the interlayer zone, MS zone, and SS zone for the forged and non-forged specimens, respectively. Seven points were analysed for elemental composition: three within the interlayer zone, two in the MS zone and SS zone near the interlayer, and two further away in the MS zone and SS zone. As shown from the figure, it can be seen a decrease of Cr element (for forged): from spot 7 (2.77 %) —> Spot 6 (2.23 %) and increasing trend start from interlayer zone at Spot 5 (3.51 %) —> Spot 4 (9.34 %) —> Spot 3 (10.80 %). Slight different trend captured for the Cr element (non-forge): the value of Cr is decrease from spot 7 (2.07 %) —> spot 6 (1.76 %). The weight percentage then, increase at spot 5 (2.5 %) —> spot 4 (10.65 %) but decrease again in spot 3 (10.44 %). For the Fe element (for forge), the decreasing trend from spot 7 (85.58 %) —> spot 6 (82.39 %), increase a little bit in spot 5 (83.71 %) then decrease quit large in spot 4 (68.14 %) —> spot 3 (67.43 %). For the non-

forge specimen, the trend for Fe element are decrease in spot 7 (87.35 %) —> spot 6 (78.67 %), static at spot 5 (82.58 %), decrease in spot 4 (78.67 %) and increase back in spot 5 (87.35 %). The amount of Fe in the interlayer zone at spots 1, 2, and 5 is comparable in both forged and non-forged specimens, however the Cr element in the same zone is much higher in the forged specimen than in the non-forged specimen. This suggests that the cold forging process causes the Cr element to diffuse from the SS zone to the MS zone. Research conducted by Gürol et al., proves that elemental diffusion between ER 316LSi and MSG 6 GZ-60 has led to the formation of a mixing zone. On the ER 316LSi side of the interface, there was a noticeable decrease in Cr, Ni, and Mo, while Fe and Cu concentrations increased [26].

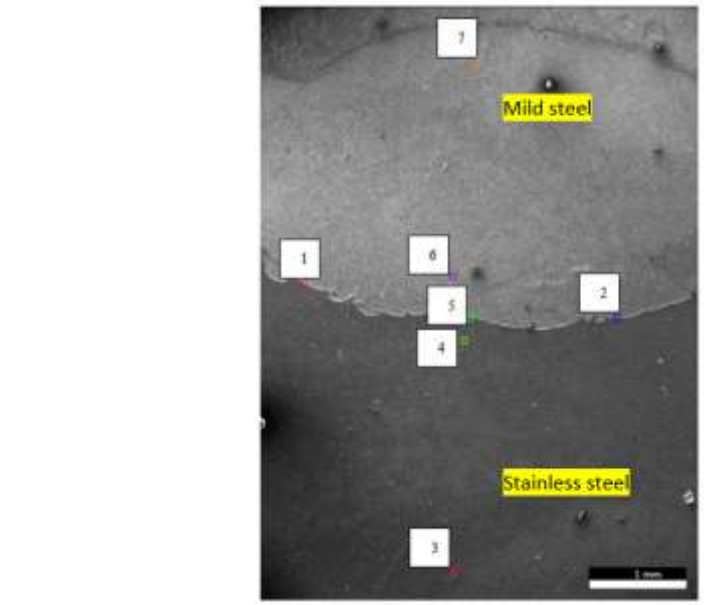

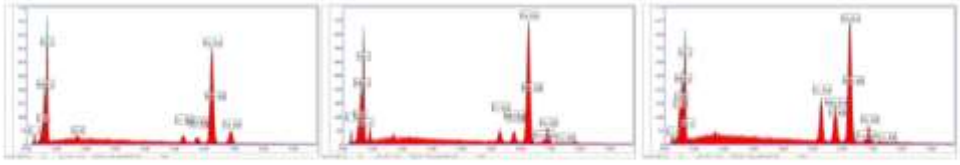

Spot 7 Spot 5 Spot 3

Elements	Weight of element at each spot (%)						
	Interlayer zone		MS zone	MS zone	Interlayer zone	SS zone	SS zone
	1	2	7	6	5	4	3
Chromium, (Cr)	4.46	5.03	2.77	2.23	3.51	9.34	10.80
Iron, (Fe)	77.90	78.12	85.58	82.39	83.71	68.14	67.43

Figure 6. EDAX element distribution for forge specimen

For spots 7 and 6, the high weight percentage of Fe indicated the presence of the MS zone, whereas the high weight percentage of Cr at spots 4 and 3 indicated the presence of the SS zone.

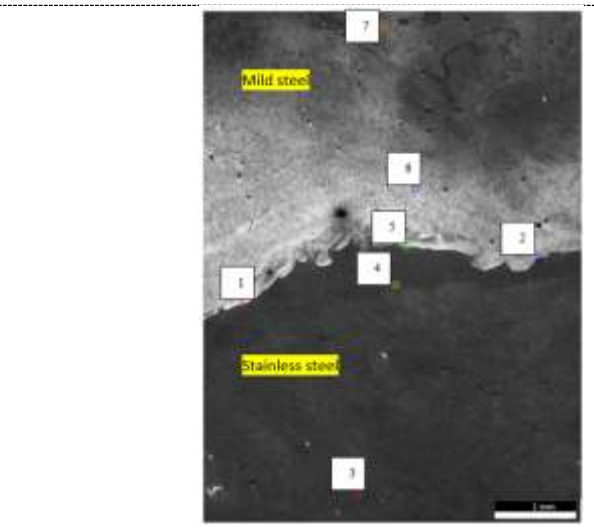

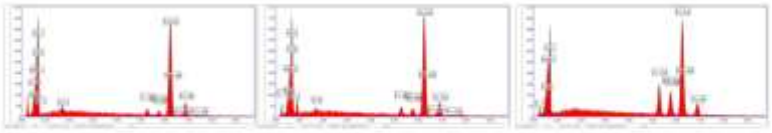

Spot 7 Spot 5 Spot 3

Elements	Weight of element at each spot (%)						
	Interlayer zone		MS zone	MS zone	Interlayer zone	SS zone	SS zone
	1	2	7	6	5	4	3
Chromium, (Cr)	2.94	3.37	2.07	1.76	2.50	10.65	10.44
Iron, (Fe)	78.71	77.48	87.35	78.67	82.58	69.62	71.89

Figure 7. EDAX element distribution for non-forge specimen.

4. Conclusions

In conclusion, the results demonstrate that cold forging significantly affects the morphology of the bimetallic deposited material in grain shape. However, the quality of the joint at the interlayer zone was slightly compromised, likely due to the setup parameters (wire feed rate and travel speed) and the condition of the first material deposited before adding the second layer. It is crucial to determine the optimal wire feed rate and travel speed to achieve the best melting point for both materials, improving interfacing. Cold forging on one side (MS zone) leads to a huge change in the grain shape of the MS zone's microstructure compared to the SS zone. The absence of Cr elements in the MS zone is significant, indicating diffusion in the bimetallic specimen. Future research should focus on finding the optimum setup for bimetallic ER308 and ER70s-6 using the Taguchi method, followed by a cold forging process on two sides (bottom and top).

5. References

[1] Kumar M B, Arivazhagan N, Tofil S, Andersson J, Kozak J and Manikandan M 2024 Influence of pulsed current GTAW-WAAM process parameters on the single layer bead geometry and multi bead multi-layer deposition of a nickel-based superalloy *Materials Today Communications* **39** 108824.

[2] Kabaldin Y, Shatagin D, Ryabov D, Solovyov A and Kurkin A 2023 Microstructure, phase composition, and mechanical properties of a layered bimetallic composite er70s-6-er309lsi obtained by the waam method *Metals* **13**(5) 851.
[3] Liu J, Miao Y, Wang Z, Zhao Y, Wu Y and Li C 2024 Improved strength in nickel aluminum bronze/steel bimetallic component fabricated using arcing-wire arc additive manufacturing with alternating deposition strategy *Journal of Manufacturing Processes* **111** 89-103.
[4] Squires L, Roberts E and Bandyopadhyay A 2023 Radial bimetallic structures via wire arc directed energy deposition-based additive manufacturing *Nature Communications* **14**(1) 3544.
[5] Sridar S, Klecka M A and Xiong W 2022 Interfacial characteristics of P91 steel-Inconel 740H bimetallic structure fabricated using wire-arc additive manufacturing *Journal of Materials Processing Technology* **300** 117396.
[6] Tomar B and Shiva S 2022 Microstructure evolution in steel/copper graded deposition prepared using wire arc additive manufacturing *Materials Letters* **328** 133217.
[7] Ayan Y and Kahraman N 2022 Fabrication and characterization of functionally graded material (FGM) structure containing two dissimilar steels (ER70S-6 and 308LSi) by wire arc additive manufacturing (WAAM) *Materials Today Communications* **33** 104457.
[8] Suárez A, Panfilo A, Aldalur E, Veiga F and Gomez P 2022 Microstructure and mechanical properties of mild steel-stainless steel bimetallic structures built using Wire Arc Additive Manufacturing *CIRP Journal of Manufacturing Science and Technology* **38** 769-773.
[9] Ahsan M R, Tanvir A N M, Seo G J, Bates B, Hawkins W, Lee C and Kim D B 2020 Heat-treatment effects on a bimetallic additively-manufactured structure (BAMS) of the low-carbon steel and austenitic-stainless steel *Additive Manufacturing* **32** 101036.
[10] Panicker C J and Senthilkumar V 2023 Rotational arc based dual wire arc additive manufacturing of low alloy steel with Nichrome inclusions for improved mechanical properties *Materials Letters* **332** 133498.
[11] Jeong T W, Cho Y T, Lee C M and Kim D H 2024 Effects of ultrasonic treatment on mechanical properties and microstructure of stainless steel 308L and Inconel 718 functionally graded materials fabricated via double-wire arc additive manufacturing *Materials Science and Engineering: A* 146298.
[12] Zhai W, Guo Y, Canturri C, Shandro R and Zhou W 2024 Wire arc additive manufacturing of ER70S-6/S355 bimetal component *Materials Science and Engineering: A* 146498.
[13] Chen Y, Zuo X, Zhang W, Hao Z, Li Y, Luo Z and Ao S 2022 Enhanced strength-ductility synergy of bimetallic laminated steel structure of 304 stainless steel and low-carbon steel fabricated by wire and arc additive manufacturing *Materials Science and Engineering: A* **856** 143984.
[14] Abioye T E, Wei C Y, Zuhailawati H and Abdullah A B 2023 Enhancing the single-track deposition quality of AISI 308L wire arc additive manufacturing via process optimization and cold forging treatment *Proceedings of the Institution of Mechanical Engineers, Part E: Journal of Process Mechanical Engineering* 09544089231215203.
[15]. Wani Z K, Abdullah A B and Hussain Z 2023 Post welding cold forging and effect on mechanical properties of low-carbon mild steel wire arc additive manufacturing *In Post-processing Techniques for Additive Manufacturing* pp 155-173 CRC Press.
[16] Casuso M, Veiga F, Suárez A, Bhujangrao T, Aldalur E, Artaza T and Lamikiz A 2021 Model for the prediction of deformations in the manufacture of thin-walled parts by wire arc additive manufacturing technology *Metals* **11**(5) 678.
[17] Duarte V R, Rodrigues T A, Schell N, Miranda R M, Oliveira J P and Santos T G 2020 Hot forging wire and arc additive manufacturing (HF-WAAM) *Additive Manufacturing* **35** 101193.
[18] Roslee M A, Abdullah A B, Hussain Z and Wani Z K 2022 Effect of Cold Forging on Wire Arc Additive Manufactured Profiles for Repair Purposes *In Advanced Maritime Technologies and Applications: Papers from the ICMAT 2021* pp 129-137 Springer International Publishing.
[19] Parvaresh B, Miresmaeili R and Yazdizadeh M 2020 Characterization of wire arc additive manufactured products: A comparison between as-deposited and inter-layer cold worked specimens *Journal of Manufacturing Processes* **57** 61-71.

[20] Gürol U, Turgut B, Kumek H, Dilibal S and Koçak M 2023 Fabrication and Characterization of Wire Arc Additively Manufactured Ferritic-Austenitic Bimetallic Structure *Metals and Materials International* 1-14.
[21] Xu N, Shen J, Hu S, Tian Y and Bi J 2021 Bimetallic structure of Ti6Al4V and Al6. 21Cu fabricated by cold metal transfer additive manufacturing via Nb interlayer added by TIG *Materials Letters* **302** 130397.
[22] Razzaq S, Pan Z X, Li H J, Ringer S P and Liao X Z 2024 Joining dissimilar metals by additive manufacturing: a review *Journal of Materials Research and Technology*.
[23] Vora J, Parikh N, Chaudhari R, Patel V K, Paramar H, Pimenov D Y and Giasin K 2022 Optimization of bead morphology for GMAW-based wire-arc additive manufacturing of 2.25 Cr-1.0 Mo steel using metal-cored wires *Applied Sciences* **12**(10) 5060.
[24] Ron T, Levy G K, Dolev O, Leon A, Shirizly A and Aghion E 2019 Environmental behavior of low carbon steel produced by a wire arc additive manufacturing process *Metals* **9**(8) 888.
[25] Mai D S, Doan T K and Paris H 2021 Wire and arc additive manufacturing of 308L stainless steel components: Optimization of processing parameters and material properties *Engineering Science and Technology, an International Journal* **24**(4) 1015-1026.
[26] Gürol U, Dilibal S, Turgut B, Baykal H, Kümek H and Koçak M 2022 Manufacturing and Characterizaton of Waam-Based Bimetallic Cutting Tool *International Journal of 3D Printing Technologies and Digital Industry* **6**(3) 548-555.